ADVANCED HEALTHCARE MATERIALS
www.advhealthmat.de

# Enhancing the Stability of COVID-19 Serological Assay through Metal–Organic Framework Encapsulation

*Yixuan Wang, Zheyu Wang, Prashant Gupta, Jeremiah J. Morrissey, Rajesh R. Naik,* and Srikanth Singamaneni**

**Enzyme-linked immunosorbent assay is widely utilized in serologic assays, including COVID-19, for the detection and quantification of antibodies against SARS-CoV-2. However, due to the limited stability of the diagnostic reagents (e.g., antigens serving as biorecognition elements) and biospecimens, temperature-controlled storage and handling conditions are critical. This limitation among others makes biodiagnostics in resource-limited settings, where refrigeration and electricity are inaccessible or unreliable, particularly challenging. In this work, metal–organic framework encapsulation is demonstrated as a simple and effective method to preserve the conformational epitopes of antigens immobilized on microtiter plate under non-refrigerated storage conditions. It is demonstrated that in situ growth of zeolitic imidazolate framework-90 (ZIF-90) renders excellent stability to surface-bound SARS-CoV-2 antigens, thereby maintaining the assay performance under elevated temperature (40 °C) for up to 4 weeks. As a complementary method, the preservation of plasma samples from COVID-19 patients using ZIF-90 encapsulation is also demonstrated. The energy-efficient approach demonstrated here will not only alleviate the financial burden associated with cold-chain transportation, but also improve the disease surveillance in resource-limited settings with more reliable clinical data.**

## 1. Introduction

COVID-19, an infectious disease caused by severe acute respiratory syndrome coronavirus-2 (SARS-CoV-2), has become a global public health challenge. As of January 2021, the disease has rapidly spread to more than 100 countries with over 85 million confirmed cases and nearly 1.8 million deaths.[1–3] Accurate, fast, and low-cost serologic assays, evaluating the presence of specific antibodies against the virus in the blood, facilitate the diagnosis and screening of symptomatic and asymptomatic patients, monitoring of the disease course, and identification of possible convalescent serum donors in resource-limited regions.[2,3]

Enzyme-linked immunosorbent assays (ELISA) is the most common method employed in serologic testing. ELISA involves surface immobilized antigens on microtiter plates to capture the SARS-CoV-2 antibodies in patient samples.[2–5] The accuracy and reliability of ELISA critically depends on the structural integrity and biofunctionality of these biomolecules. However, due to the poor stability of proteins under ambient and elevated temperatures, both antibodies and antigens are prone to lose their structure and functionalities.[6–9] More importantly, antigens immobilized on solid surface (e.g., microtiter plate) exhibit lower stability under non-refrigerated conditions compared to those in buffer solution.[10–12] Therefore, "cold-chain" system is necessary to maintain the stability and ensure the performance of these assays following the storage, transportation, and handling of the diagnostic reagents. Unfortunately, besides the extra financial burden, cold chain systems are not feasible in developing parts of the world and resource-limited settings, where refrigeration and electricity are not available, but disease surveillance and control are critically needed.[13–18] Therefore, it is imperative to develop a low-cost and facile, refrigeration-free technology to preserve the biorecognition capability of antigens immobilized on solid surface and disease-specific antibodies in patient samples, providing reliable and accurate serologic assays for resource-limited settings.

Metal–organic frameworks (MOFs), comprised of polynuclear metal clusters or ions bridged by organic ligands, have increasingly received wide interests.[19–23] MOFs exhibit extremely large surface area, tunable porosity, diverse chemical functionality,

Y. Wang, Z. Wang, P. Gupta, S. Singamaneni
Department of Mechanical Engineering and Materials Science
Institute of Materials Science and Engineering
Washington University in St. Louis
Saint Louis, MO 63130, USA
E-mail: singamaneni@wustl.edu

J. J. Morrissey
Department of Anesthesiology
Washington University in St. Louis
St. Louis, MO 63110, USA

J. J. Morrissey, S. Singamaneni
Siteman Cancer Center
Washington University School of Medicine
St. Louis, MO 63130, USA

R. R. Naik
711th Human Performance Wing
Air Force Research Laboratory
Wright Patterson Air Force Base
Dayton, OH 45433, USA
E-mail: rajesh.naik@us.af.mil

The ORCID identification number(s) for the author(s) of this article can be found under https://doi.org/10.1002/adhm.202100410

**DOI: 10.1002/adhm.202100410**

 

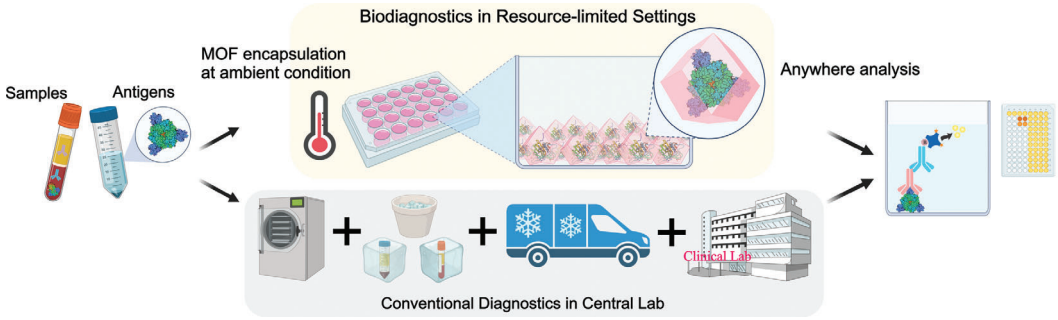


**Figure 1.** Schematic illustration depicting the concept of MOF-based bioassay preservation.

and high thermal stability,[21–23] making them highly attractive for biomineralization,[24] encapsulation,[25] biosensors,[26] drug delivery,[27] gas storage,[28] and catalysis.[29] Among these applications, of particular interest is the encapsulation of biomolecules via in situ growth of MOF crystals in the presence of biomolecules at room temperature under mild aqueous conditions.[24–26,30–33] MOFs serve as rigid exoskeletons, preserving the structure and biofunctionality of embedded molecules against denaturation/degradation under elevated temperature, organic solvents, and proteolytic conditions.[24,26] Although MOF encapsulation has been demonstrated for preserving enzymes, soluble proteins/biomarkers and antibodies in biosensors, preserving immobilized antigens in an immunoassay has not been demonstrated. In contrast to antibodies, antigens are more sensitive to environmental conditions after surface immobilization, necessitating effective biopreservation methods. Changes in their secondary and tertiary structure can result in the loss of conformational epitopes and consequently the antibody recognition, thus compromising the accuracy and sensitivity of the assay. We hypothesize that MOFs are a promising class of materials for preserving the structure and biofunctionality of surface-bound antigens (i.e., recognition elements) and antibodies (i.e., target analytes) in biospecimen, thus enabling reliable and accurate SARS-CoV-2 serologic assays even in resource-limited regions.

In this study, we demonstrate zeolitic imidazole framework-90 (ZIF-90) as a simple and effective encapsulation method for preserving the biorecognition capabilities of both SARS-CoV-2 antibodies in patient serum and substrate-immobilized SARS-CoV-2 antigens under elevated temperature and proteolytic conditions. ZIF-90 was in situ grown on SARS-CoV-2 nucleocapsid protein (N protein) and S1 subunit (S1) immobilized on microtiter plate. The SARS-CoV-2 antibodies in patient serum were encapsulated within ZIF-90 crystals by mixing the serum samples with MOF precursors. The biofunctionality of embedded biomolecules were restored through a mild aqueous rinsing step to completely remove ZIF-90 protective layer before implementing the serologic assay. Encapsulation with ZIF-90 significantly improved the stability of surface-bound antigens and antibodies with over 90% of recognition ability after storage at high temperature (up to 60 °C) and exposure to proteases. Overall, the MOF encapsulation method broadly extends the COVID-19 diagnostic, screening and surveillance ability to underserved populations and resource-limited settings (**Figure 1**).

## 2. Result and Discussion

A typical SARS-CoV-2 serologic ELISA involves the immobilization of spike glycoprotein protein (S1 subunit) and nucleocapsid protein (N protein) as antigens, selective capture of corresponding antibodies in patient serum, followed by binding of secondary antibodies and labeled by enzymatic reporters (**Figure 2**A and Figure S1, Supporting Information). N protein is the most abundant protein in SARS-CoV-2 virion.[34] S protein, comprised of two subunits (S1 and S2), is a type-I transmembrane glycoprotein that plays an important role in mediating viral infection,[35] where the S1 subunit binds to the cellular receptors through its receptor-binding domain.[2,35] The antibodies against N protein are usually more abundant compared to those against S1, while the latter better correlate with the protection against the disease compared to the former.[36,37]

To preserve the surface-bound N and S1 antigens for bioassays, we first investigate the feasibility of in situ growth and dissociation of ZIF-90 on the surface-bound antigens. Owing to the rich functional groups, proteins serve as nucleating sites for the fast nucleation and growth of ZIF-90 crystals.[24,38] ZIF-90 crystals render tight encapsulation of the antigens, and minimize the changes in their secondary and tertiary structure even under harsh environmental conditions. The ZIF-90 protective layer was formed by incubating the antigen-coated microtiter plate with the precursor solution (a mixture of zinc nitrate and 2-imidazolatecarboxyaldehyde) for 1 h. After storing the ZIF-90 protected plate for a desired duration at desired temperature, the protective layer was removed by EDTA/phosphate buffer solution (pH $\approx$ 5.4) before performing the bioassay (see Experimental Section for details). The ZIF-90 dissociation occurs due to the loss of coordination between organic ligands and zinc ions at the acidic condition.[39,40] The ZIF-90 film was characterized by atomic force microscope (AFM) and scanning electron microscope (SEM). AFM images revealed distinct morphology of antigen-coated plate before and after ZIF-90 coating (Figure 2B). With ZIF-90 coating, a dense grainy morphology (Figure 2B(i)) was observed and the AFM scratch test on silicon indicated the thickness of ZIF-90 layer to be 40 $\pm$ 5 nm (Figure S2, Supporting Information). SEM images further confirmed the distinct morphology of MOF-coated plate (Figure 2C(i)) compared to the plate without MOF coating (Figure 2C(ii)). The growth and removal of ZIF-90 layers was also confirmed by Raman spectroscopy (Figure 2D). Raman spectra obtained from ZIF-90 coated plate

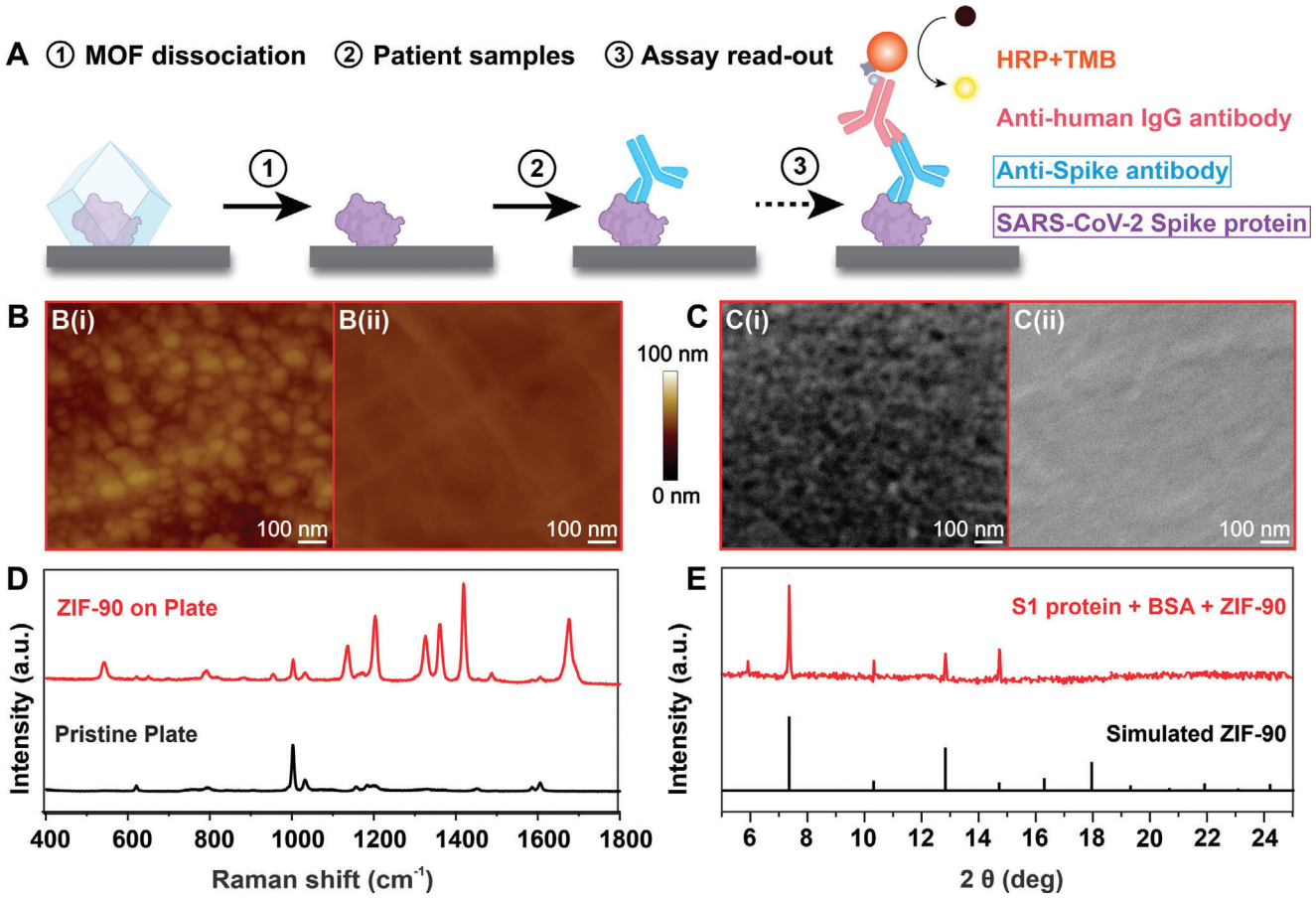


**Figure 2.** A) Schematic depicting ZIF-90 removal and assay procedure. B) AFM images for antigen-coated microtiter plate surface with ZIF-90 (B(i)) and without ZIF-90 (B(ii)). C) SEM images for antigen-coated microtiter plate surface with ZIF-90 (C(i)) and without ZIF-90 (C(ii)). D) Raman spectra obtained from antigen-coated microtiter plate before and after growing ZIF-90 layer. E) XRD pattern obtained from ZIF-90 encapsulated antigens on silicon substrate and simulated ZIF-90 XRD patterns.

exhibited bands originating from the 2-imidazolatecarboxyaldehyde ring vibration at 1135 and 1202 $cm^{-1}$. Other Raman bands were observed at 1325 ($\delta_{H-CO}$), 1361 ($\delta_{C-H}$), and 1419 $cm^{-1}$ ( $\upsilon_{C2-N1}$).[41] Raman band at 1675 $cm^{-1}$ obtained from plate with ZIF-90 coated antigens can be ascribed to amide moieties of the proteins. The shift in the amide band from 1650–1655 $cm^{-1}$ to 1675 $cm^{-1}$ suggests a slight change of coordination environment due to the interactions between protein and ZIF-90.[42,43] X-ray diffraction (XRD) also confirmed the formation of ZIF-90 crystals on the antigen-coated plate (Figure 2E). XRD peak positions of the antigen-encapsulating ZIF-90 crystals on silicon substrate were mostly identical with the simulated XRD pattern of ZIF-90, which confirmed the in situ formation of ZIF-90 on the ELISA plate. Additional surface characterization of the microtiter plate by AFM, SEM, and Raman at different steps further confirm the growth and dissociation of the ZIF-90 crystals (Figure S3, Supporting Information)

We set out to investigate the effect of the growth and removal process of ZIF-90 on specificity and sensitivity of SARS-CoV-2 serological assay. To assess the preservation efficacy of ZIF-90 coatings, we compared the limit-of-detection (LOD) and signal intensity (i.e., optical density at 450 nm) attained from microtiter plates stored in different conditions with those obtained from plates stored under "gold standard" refrigerated condition (i.e., stored at −20 °C with sucrose protection). LOD of ELISA, a commonly used metric for measuring assay sensitivity, was defined as the concentration corresponding to the mean+3×standard deviation ($\sigma$) of the lowest concentration point (or blank). To explore the possible influence of MOF coating and removal process, ZIF-90 layer was grown on antigen-coated plate, followed by removal of the overlayer. Serial dilutions of antibodies with known concentration were employed as standards. The LOD of freshly prepared (positive control) plate and ZIF-90 encapsulated microtiter plate was found to be 7.06 and 7.54 pg $mL^{-1}$ (Figure S4, Supporting Information), respectively, indicating that the encapsulation and removal processes have negligible effect on the biofunctionality of surface-bound antigens.

Next, we investigate the efficacy of ZIF-90 in preserving the surface-bound SARS-CoV-2 antigens against harsh environmental conditions (at 40 °C up to 32 days, or exposure to proteases), simulating transport and long-term storage conditions that would normally lead to loss of conformational epitopes of these biorecognition elements. The S1 protein coated plates with and without ZIF-90 encapsulation were stored at 40 °C for 8 days,

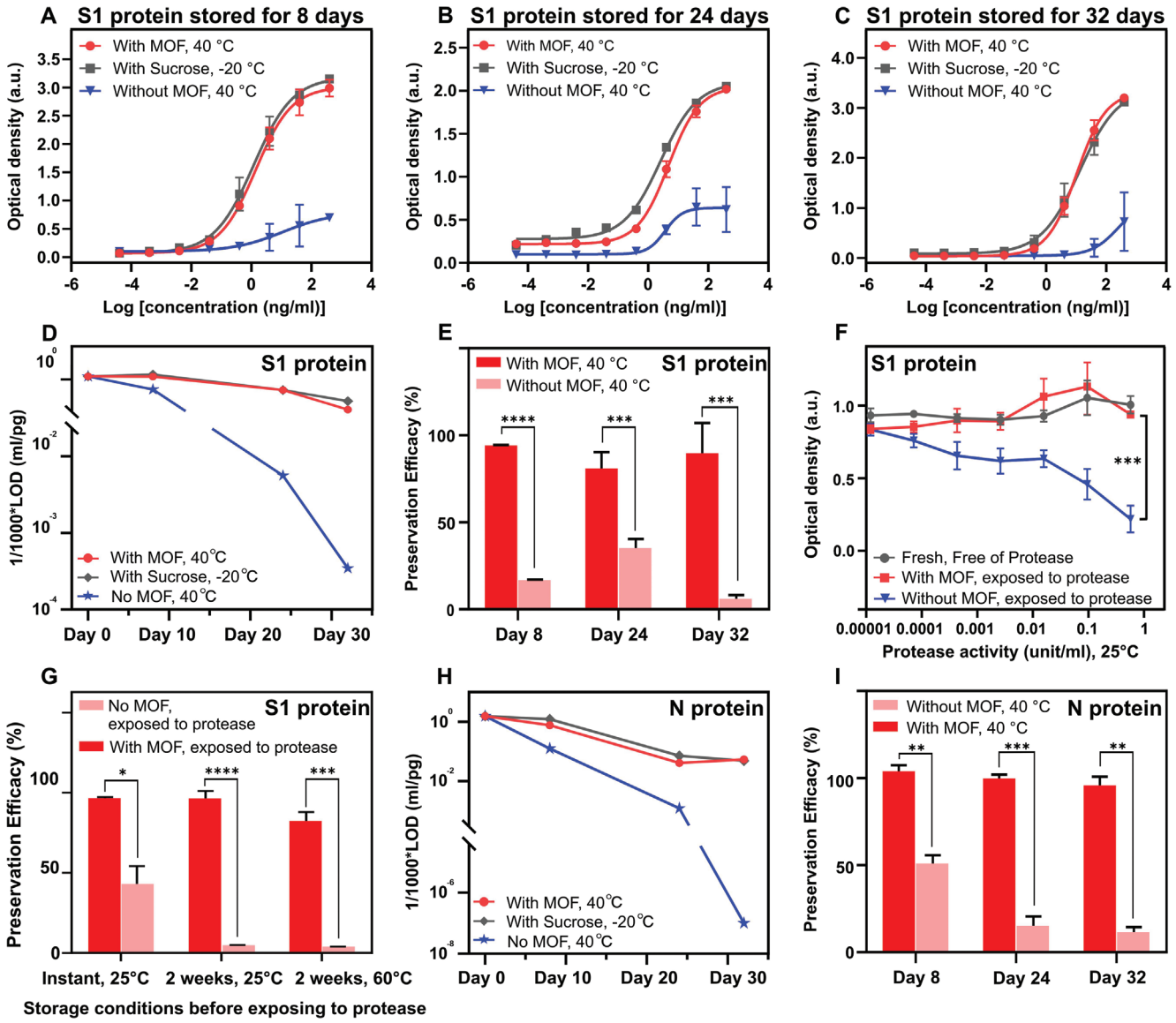


**Figure 3.** ELISA standard curves obtained from microtiter plates coated with SARS-CoV-2 S1 protein and stored under different conditions for A) 8 days, B) 24 days, and C) 32 days. D) Preservation efficacy as calculated from the OD values in the linear range of ELISA standard curves of SARS-CoV-2 S1 protein-coated microtiter plates. E) Comparison of LODs of SARS-CoV-2 S1 protein coated plates stored under different conditions. F) OD values obtained from SARS-CoV-2 S1 protein-coated plates after treatment with different concentrations of proteases. G) Preservation efficacy of ZIF-90 protected plates after thermal treatment and then exposing to protease. H) Comparison of LODs of SARS-CoV-2 N protein coated microtiter plates stored under different conditions. I) Preservation efficacy as calculated from the OD values in the linear range of ELISA standard curves of SARS-CoV-2 N protein precoated plates. E-G, I) n=2, *P < 0.05, **P < 0.01, ***P < 0.005, ****P < 0.0001, analyzed by unpaired t-test. Data represent mean ± s.d.

24 days, and 32 days, and plates stored with sucrose protection at −20 °C were used as "gold standard" reference (**Figure 3**A–C). After 32 days of storage at 40 °C, the LOD of ZIF-90 protected microtiter plate was found to be 39.4 pg $mL^{-1}$ for S1 protein, which is comparable to the LOD of the plates stored under refrigeration (14.2 pg $mL^{-1}$). The LOD of microtiter plate with ZIF-90 encapsulation was found to be around 80-fold lower for S1 protein compared to that without ZIF-90 protection after storage at 40 °C for 32 days (Figure 3D). We calculated the preservation efficacy of ZIF-90 by comparing the OD values obtained from linear region of the standard curve under different storage conditions (Figure 3A–C). Preservation efficacy (%) is calculated as the percentage of the OD obtained from a restored microtiter plate after storage under different conditions compared to the OD obtained with the same batch of freshly fabricated microtiter plate. After 8 days of storage, ZIF-90 encapsulated plates exhibited only ≈5% loss in sensitivity for surface-bound S1 proteins, which is significantly lower compared to the nearly 50% loss in sensitivity for plates without ZIF-90 (Figure 3E). Significantly, after storage for 32 days, ZIF-90 protected microtiter plates exhibited sensitivity close to that of the plates stored at −20 °C with sucrose protection, with a preservation efficacy of 93%. In contrast, plates stored

under identical conditions without MOF protection exhibited nearly 90% loss in sensitivity (Figure 3E).

In addition to storage at elevated temperature, we have assessed the efficacy of ZIF-90 in preserving the surface-bound antigens against proteolytic conditions (Figure 3F,G). Proteases can cause antigen degradation by cleaving the peptide bonds, thus compromising their biorecognition ability.[44] After exposure to protease solution (protease from *Streptomyces griseus*) at various concentrations for 60 min, we noted that surface-bound S1 protein retained less than 20% of biorecognition capability (as determined from the OD values in the linear region of the standard curve) for protease activity of 0.525 unit $mL^{-1}$ (Figure 3F). Remarkably, surface-bound S1 protein with ZIF-90 protection retained over 90% biorecognition ability under protease activity (0.525 unit $mL^{-1}$), which is similar to pristine surface-bound S1 protein without protease treatment (Figure 3F). Furthermore, we investigated the protease shielding ability of ZIF-90 after thermal treatment. Surface-bound S1 protein stored at room temperature and 60 °C for 2 weeks were exposed to proteases for 1 h. Protease treatment (0.0875 unit $mL^{-1}$) of the unprotected surface-bound S1 protein exhibited less than 50% of biorecognition capacity (Figure 3G). ZIF-90 encapsulated antigens, after storage at room temperature for 2 weeks followed by protease treatment for 1 h, retained a recognition capability of 96%, whereas antigens subjected to identical harsh conditions without ZIF-90 encapsulation exhibited nearly complete loss (less than 5% retained) of biorecognition ability (Figure 3G). Surface-bound S1 protein stored at 60 °C for 2 weeks and exposed proteases for 1 h retained above 82% of recognition capability with ZIF-90 protection, while less than 5% of recognition ability was retained without ZIF-90 protection (Figure 3G). These stress tests indicate that ZIF-90 is capable of shielding S1 protein from both proteases and elevated temperature.

In addition to S1 protein, we investigated the stabilization of N protein using similar strategy. For surface-bound N protein stored at 40 °C for 32 days, the LOD of ZIF-90 protected microtiter plates was calculated to be 18.8 pg $mL^{-1}$, which is comparable to "gold standard" refrigeration method (20.8 pg $mL^{-1}$) (Figure 3H). Furthermore, ZIF-90 protected surface-bound N protein retained over 90% of recognition ability after storing at 40 °C for 32 days, whereas less than 12% of recognition capability was retained without ZIF-90 protection (Figure 3I). The consistent results of S1 protein and N protein indicate the universality of the ZIF-90 encapsulation in preserving the surface-bound antigens on microtiter plates.

Next, we sought to demonstrate the applicability of ZIF-90 encapsulated microtiter plates in analyzing patient plasma samples. Compared to purified antibodies (employed as standard in the experiments described above), human plasma sample represents a complex biological matrix, comprised of various biomolecules such as antibodies, enzymes, and metabolites that can interfere with diagnostics assays. This study utilized plasma samples obtained from the Washington University School of Medicine's COVID-19 biorepository through informed consent. All patients have been tested positive for SARS-CoV-2 with RT-PCR before serum collection. Our studies were conducted under approval by the Washington University Institutional Review Board under IRB 202004097. We set out to evaluate the ability of ZIF-90 protected surface-bound antigens to recognize antibodies in plasma samples obtained from COVID-19 patients. Eight plasma samples from COVID-19 patients (#13, #14, #15, #17, #25, #26, #29, and #30) were tested for antibodies against SARS-CoV-2 using S1 protein and N protein (antigens) as biorecognition elements. Surface-bound S1 protein on ELISA plates with and without ZIF-90 protection were stored at 40 °C for 8, 24, and 32 days. Plates protected with sucrose at −20 °C were employed as reference. Before testing, all patient samples were diluted with 6000-fold in phosphate buffered saline (PBS), to ensure that the final testing concentration is in the linear range of standard curve (standard curves shown in Figure 3A–C). ZIF-90 protected antigens (S1 protein and N proteins) immobilized on microtiter plate retained above 95% of preservation efficacy after 8 days and above 90% of preservation efficacy after 32 days stored at 40 °C (**Figure 4**). In stark contrast, antigens on the plates without ZIF-90 protection show less than 60% of preservation efficacy after 8 days of storage and less than 15% of preservation efficacy after storage for 32 days at 40 °C (Figure 4). Such stable biodiagnostic performance of ZIF-90 protected microtiter plates coated with desired antigens indicate the feasibility of harnessing this encapsulation approach in deploying the serological assay in resource-limited settings

Next, we set out to determine if ZIF-90 could be used to stabilize plasma as a complementary approach to deploy biodiagnostics in resource-limited settings. The preservation and testing methods are based on the protocols from our previous works with slight modifications.[38] As illustrated in **Figure 5**A, plasma samples from COVID-19 patients were first mixed with 2-imidazolatecarboxyaldehyde (200 mM) followed by zinc nitrate solution (200 mM). After 40 min of incubation at room temperature, plasma containing SARS-CoV-2 antibodies encapsulated in ZIF-90 crystals were collected by drying the solution on Whatman 903 paper strip (Figure 5A). The ZIF-90 nanocrystals encapsulating the plasma components were characterized by SEM, Raman, and XRD. After encapsulation of patient plasma samples, the SEM images exhibit sodalite morphology (with particle size of 2–10 μm) (Figure 5B). Raman bands at 1137, 1205, and 1329–1419 $cm^{-1}$ correspond to C═O stretching vibration of 2-imidazolatecarboxyaldehyde and the peak at 1675 $cm^{-1}$ can be ascribed to amide bonds of the encapsulated proteins (Figure 5C). XRD pattern of plasma-embedded ZIF-90 crystals display the characteristic peaks corresponding to pristine ZIF-90 crystals (Figure 5C).

The thermal stability of ZIF-90 encapsulated plasma sample was evaluated by storing plasma samples with and without ZIF-90 encapsulation at 40 °C for over 3 weeks, which serves as a surrogate for harsh transport/storage condition. The preservation efficacy was then calculated by comparing the amounts of antibodies detected with ZIF-90 protection with that in the pristine samples stored under refrigeration. For all 8 patients (#13, #14, #15, #17, #25, #26, #29, and #30), the samples with ZIF-90 encapsulation resulted in more than 80% preservation efficacy after 3 weeks stored at 40 °C, whereas less than 15% preservation efficacy was observed in samples without ZIF-90 encapsulation (Figure 5D and 5E).

Finally, we set out to investigate the efficacy of ZIF-90 in preserving anti-human IgG antibodies. The thermal stability of ZIF-90 encapsulated anti-human IgG antibodies was evaluated by storing the anti-human IgG with and without ZIF-90

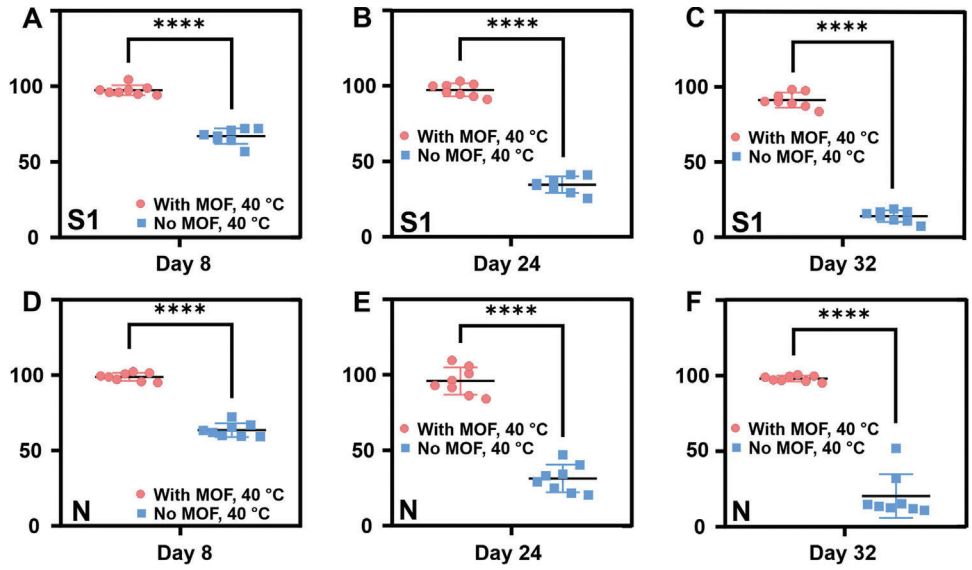


**Figure 4.** Preservation efficacy of surface-bound (A-C) S1 protein and (D-F) N protein stored for different durations with ZIF-90 andwithout ZIF-90 encapsulation. (A-F) n=8, ****P < 0.0001, analyzed by unpaired t-test.

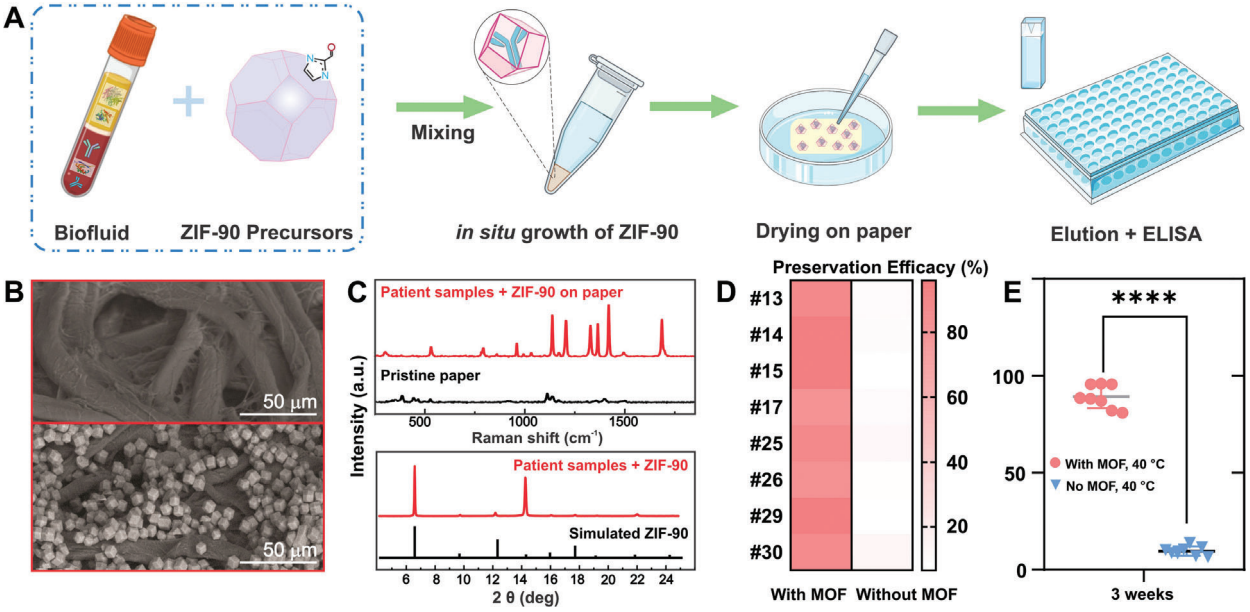


**Figure 5.** A) ZIF-90 encapsulation procedures of COVID-19 patient samples. B) SEM image of pristine paper substrate (top) and after drying plasma encapsulating ZIF-90 crystals on the surface (bottom). C) Raman spectra obtained from pristine paper substrate and after drying plasma encapsulating ZIF-90 crystals on the surface (top); XRD patterns of ZIF-90 encapsulated patient sample and simulated ZIF-90 pattern (bottom). D)Heat map and E) statistical analysis of the preservation efficacy of plasmasamples from COVID-19 patients with and without ZIF-90 encapsulation afterstorage at 40 °C for 3 weeks. (E) n=8, ****P < 0.0001, analyzed by unpaired t-test.

encapsulation at 40 °C for 8 days. The preservation efficacy was then calculated by employing them as secondary antibodies in SARS-CoV-2 serologic ELISA. Specifically, we compared the concentration of SARS-CoV-2 antibodies detected using stored (at 40 °C for 8 days) anti-human IgG with and without ZIF-90 encapsulation with that obtained using anti-human IgG stored at 4 °C (positive control). For the two patient samples (#14 and #29) tested, ZIF-90 encapsulation exhibited more than 90% preservation efficacy after 8 days stored at 40 °C, whereas less than 60% preservation was observed in samples without ZIF-90 encapsulation (Figure S5, Supporting Information). Overall, ZIF-90 encapsulation method presented in this work serves as a simple and robust strategy for preserving biodiagnostic capability of surface-bound antigens and anti-human IgG antibodies that are employed as diagnostic reagents, and antibodies in patient samples.

## 3. Conclusions

In summary, for the first time, we have demonstrated the ZIF-90 encapsulation of antigens immobilized on a microtiter plate and its role as an exoskeleton in protecting the biorecognition ability of antigens against harsh environment conditions (including elevated temperature (up to 60 °C), protease, and long-term storage without refrigeration). The ZIF-90 protected surface-bound antigens at elevated temperature retained above 80% biorecognition capability after storage at 40 °C for over one month, which is comparable to existing "gold standard" methods (storage at −20 °C with sucrose protection). In addition, we have demonstrated that ZIF-90 encapsulation can preserve SARS-CoV-2 antibodies in patient plasma samples at 40 °C for over 3 weeks, with preservation efficacy comparable to that of the refrigeration method. The high thermal stability of antigens and antibodies rendered by ZIF-90 encapsulation can extend the benefits of biodiagnostics to resource-limited settings and underserved populations. MOF encapsulation can potentially eliminate the need for cold-chain in biodiagnostics and decrease the reliance on centralized labs, improving the overall effectiveness in utilizing the advances in ultrasensitive biodiagnostics in controlling the outbreaks of infectious diseases and early detection and monitoring of other pathological conditions.

## 4. Experimental Section

*Chemicals*: Recombinant SARS-CoV-2 Nucleocapsid protein (Cat.# 230 30164) and Recombinant SARS-CoV-2 S1 subunit (Cat.# 230 01102) were purchased from Raybiotech, Inc. SARS-CoV-2 Nucleocapsid (N) protein (Rabbit) antibody (Cat.# 600-401-MS4) and SARS-CoV-2 spike (S1) protein (Rabbit) antibody (Cat.# 600-401-MS8), biotinylated anti-human IgG (H&L) (Rabbit) (Cat.# 609 4617), and biotinylated donkey anti-rabbit IgG (Cat.# 616 4102) were purchased from Rockland, Inc. Streptavidin-HRP and TMB substrate were purchased from R&D System. Zinc nitrate, 2-imidazolecarboxaldehyde (ICA), ethylenediaminetetraacetic acid (EDTA), Tween 20, sodium phosphate monobasic, sodium phosphate dibasic, sodium formate, and protease (protease from *S. griseus*) were purchased from Sigma-Aldrich. This study utilized plasma samples obtained from the Washington University School of Medicine's COVID-19 biorepository through informed consent. All patients have tested positive for SARS-CoV-2 with RT-PCR before serum collection. Our studies were conducted under approval by the Washington University Institutional Review Board under IRB 202004097.

*Encapsulation of Proteins on Microtiter Plate with ZIF-90 Films*: Microtiter plate was first coated with 2 μg $mL^{-1}$ S1 protein or N protein in PBS at room temperature for overnight and blocked with 1% BSA in PBS for 3 h. For ZIF-90 encapsulation, ICA (200 mM) and zinc nitrate solution (200 mM) was simultaneously added into each well and agitated for 2 h. Subsequently after aspiration of liquid and drying with a stream of nitrogen, the plates were stored at 25 and 40 °C for different time intervals and subjected to other harsh conditions as described in the main text.

*Encapsulation of Proteins in Patient Serum with ZIF-90 Crystals*: Patient serum (1.2 μL) were first diluted 60-times with PBS before being mixed with ICA (320 μL) and 80 μL of zinc nitrate solution simultaneously. The final concentration of ICA and zinc nitrate is 200 mM. After 40 min of incubation at room temperature (20–23 °C), mixture solution was pipetted onto Whatman 903 paper strip, followed by air-drying. The ratio between fluid volume and area of Whatman paper was maintained ≈50 μL $cm^{-2}$ to avoid liquid leakage from paper strip. After air-drying, strips were sealed in Petri dishes and stored at 40 °C for 3 weeks.

*Protein Recovery and ELISA*: To recover embedded proteins from ZIF-90 crystals, MOF dissociation buffer (0.1 M phosphate buffer with 200 mM EDTA and 0.1% Tween20 at pH 5.4) was added to each of the wells and subjected to orbital shaking for 15 min, followed by aspirating the buffer and washing with PBST (1× PBS, 0.05% Tween20). Serial dilutions of rabbit anti SARS-CoV-2 Spike or Nucleocapsid protein with known concentration were used as standards and applied on the eluted plates for 2 h. The concentrations of anti-nucleocapsid (N) protein range from 160 fg $mL^{-1}$ to 1.6 mg $mL^{-1}$, while the concentrations of anti-spike protein antibody range from 40 fg $mL^{-1}$ to 0.4 mg $mL^{-1}$. After washing with PBST, plate was incubated with biotin labeled anti rabbit IgG (1:2000 in 1% BSA-PBST) for another 2 h, followed by the addition of HRP-labeled streptavidin for 20 min. 100 μL of substrate solution was subsequently added to each well and the reaction was stopped with 50 μL $H_2SO_4$ (2 N). Optical density of each well was determined immediately using a microplate reader set to 450 nm. The assay for patient serum samples was similar except that biotin-labeled anti human IgG was used as secondary antibody.

To recover embedded proteins from ZIF-90 crystals, the paper strips were eluted in a cuvette containing 1 mL of elution buffer (0.1 M phosphate buffer with 200 mM EDTA and 0.1% Tween20 at pH 5.4) with gentle shaking for 45 min. The elution solution was then assayed by ELISA for SARS-CoV-2 specific antibody. Microtiter plate was coated with 2 μg $mL^{-1}$ S1 protein or N protein in PBS at room temperature for overnight and blocked with 1% BSA in PBS for 3 h before being applying the eluted patient serum. Subsequent assay steps are similar to the abovementioned protocol.

*Material Characterization*: AFM images were collected by Dimension 3000 AFM (Digital instruments) in light tapping mode. The XRD measurements of the samples were recorded on a Bruker D8-Advance X-ray powder diffractometer using Cu K$\alpha$ radiation ($\lambda = 1.5406$ Å) with scattering angles ($2\theta$) of 5°–25°. The Raman spectra were obtained using a Renishaw inVia confocal Raman spectrometer mounted on a Leica microscope with a 50× objective and a 785 nm wavelength diode laser was employed as the illumination source. SEM images were obtained using Thermo Scientific Quattro S Environmental SEM.

*Statistical Analysis*: Statistical analyses were performed by GraphPad Prism (8.0) and evaluated by unpaired two-tailed t-test with Welch's correction. Statistical Significance of data was calculated at 95% confidence intervals. P values of 0.05 or less were considered statistically significant. Data presented as mean + SD or plots. We employed polynomial fit to calculate the LOD in the standard curves of bioassay. The LOD is defined as the analyte concentration corresponding to the mean optical density of blank plus three times of its standard deviation. Origin 2018 was used for calculating the LOD.

## Supporting Information

Supporting Information is available from the Wiley Online Library or from the author.

## Acknowledgements

The authors acknowledge the support from National Cancer Institute-Innovative Molecular Analysis Technologies (R21CA236652). The authors thank the Nano Research Facility (NRF) and Institute for Materials Science and Engineering (IMSE) at Washington University in St. Louis for providing access to characterization facilities. This study utilized plasma samples obtained from the Washington University School of Medicine's COVID-19 biorepository through informed consent, developed and maintained by Jane O'Halloran, MD, Ph.D.; Rachel Presti, MD, Ph.D., Charles Goss, Ph.D., and Phillip Mudd, MD, Ph.D. The biorepository is supported by: the Barnes-Jewish Hospital Foundation; the Siteman Cancer Center grant P30 CA091842 from the National Cancer Institute of the National Institutes of Health; and the Washington University Institute of Clinical and Translational Sciences grant UL1TR002345 from the National Center for Advancing Translational Sciences of the National Institutes of Health. The studies were conducted under approval by the Washington University Institutional Review Board under IRB 202004097.

## Conflict of Interest

The authors declare no conflict of interest.

## Data Availability Statement

The data that support the findings of this study are available from the corresponding author upon reasonable request.

## Keywords

enzyme-linked immunosorbent assays, metal–organic frameworks, preservation, resource-limited settings, SARS-CoV-2

Received: March 4, 2021
Revised: June 16, 2021
Published online: July 23, 2021

[1] M. Poudineh, C. L. Maikawa, E. Y. Ma, J. Pan, D. Mamerow, Y. Hang, S. W. Baker, A. Beirami, A. Yoshikawa, M. Eisenstein, S. Kim, J. Vuckovic, E. A. Appel, H. T. Soh, *Nat. Biomed. Eng.* **2020**, *5*, 53.
[2] F. Amanat, D. Stadlbauer, S. Strohmeier, T. H. O. Nguyen, V. Chromikova, M. McMahon, K. Jiang, G. A. Arunkumar, D. Jurczyszak, J. Polanco, M. Bermudez-Gonzalez, G. Kleiner, T. Aydillo, L. Miorin, D. S. Fierer, L. A. Lugo, E. M. Kojic, J. Stoever, S. T. H. Liu, C. Cunningham-Rundles, P. L. Felgner, T. Moran, A. García-Sastre, D. Caplivski, A. C. Cheng, K. Kedzierska, O. Vapalahti, J. M. Hepojoki, V. Simon, F. Krammer, *Nat. Med.* **2020**, *26*, 1033.
[3] S. E. F. Yong, D. E. Anderson, W. E. Wei, J. Pang, W. N. Chia, C. W. Tan, Y. L. Teoh, P. Rajendram, M. P. H. S. Toh, C. Poh, V. T. J. Koh, J. Lum, N. A. M. Suhaimi, P. Y. Chia, M. I. C. Chen, S. Vasoo, B. Ong, Y. S. Leo, L. Wang, V. J. M. Lee, *Lancet Infect. Dis.* **2020**, *20*, 809.
[4] G. A. Posthuma-Trumpie, J. Korf, A. van Amerongen, *Anal. Bioanal. Chem.* **2009**, *393*, 569.
[5] A. J. Johnson, D. A. Martin, N. Karabatsos, J. T. Roehrig, *J. Clin. Microbiol.* **2000**, *38*, 1827.
[6] A. W. Vermeer, W. Norde, *Biophys. J.* **2000**, *78*, 394.
[7] C. N. Pace, S. Treviño, E. Prabhakaran, J. M. Scholtz, *Philos. Trans. R. Soc., B* **2004**, *359*, 1225.
[8] B. E. Turk, L. L. Huang, E. T. Piro, L. C. Cantley, *Nat. Biotechnol.* **2001**, *19*, 661.
[9] J. F. Brandts, L. Hunt, *J. Am. Chem. Soc.* **1967**, *89*, 4826.
[10] D. Kim, A. E. Herr, *Biomicrofluidics* **2013**, *7*, 041501.
[11] J. S. Bee, D. Chiu, S. Sawicki, J. L. Stevenson, K. Chatterjee, E. Freund, J. F. Carpenter, T. W. Randolph, *J. Pharm. Sci.* **2009**, *98*, 3218.
[12] B. Saha, T. H. Evers, M. W. J. Prins, *Anal. Chem.* **2014**, *86*, 8158.
[13] J. R. Choi, J. Hu, S. Feng, W. A. B. Wan Abas, B. Pingguan-Murphy, F. Xu, *Biosens. Bioelectron.* **2016**, *79*, 98.
[14] D. Mabey, R. W. Peeling, A. Ustianowski, M. D. Perkins, *Nat. Rev. Microbiol.* **2004**, *2*, 231.
[15] C. Chaigneau, T. Cabioch, K. Beaumont, F. Betsou, *Clin. Chem. Lab. Med.* **2007**, *45*, 1390.
[16] M. J. Evans, J. H. Livesey, M. J. Ellis, T. G. Yandle, *Clin. Biochem.* **2001**, *34*, 107.
[17] C. D. Chin, V. Linder, S. K. Sia, *Lab Chip* **2007**, *7*, 41.
[18] P. Yager, T. Edwards, E. Fu, K. Helton, K. Nelson, M. R. Tam, B. H. Weigl, *Nature* **2006**, *442*, 412.
[19] O. M. Yaghi, M. O'Keeffe, N. W. Ockwig, H. K. Chae, M. Eddaoudi, J. Kim, *Nature* **2003**, *423*, 705.
[20] W. Morris, C. J. Doonan, H. Furukawa, R. Banerjee, O. M. Yaghi, *J. Am. Chem. Soc.* **2008**, *130*, 12626.
[21] H. Furukawa, K. E. Cordova, M. O\textquoterightKeeffe, O. M. Yaghi, *Science* **2013**, *341*, 1230444.
[22] M. L. Foo, R. Matsuda, S. Kitagawa, *Chem. Mater.* **2014**, *26*, 310.
[23] G. Lu, O. K. Farha, W. Zhang, F. Huo, J. T. Hupp, *Adv. Mater.* **2012**, *24*, 3970.
[24] K. Liang, R. Ricco, C. M. Doherty, M. J. Styles, S. Bell, N. Kirby, S. Mudie, D. Haylock, A. J. Hill, C. J. Doonan, P. Falcaro, *Nat. Commun.* **2015**, *6*, 7240.
[25] M. A. Luzuriaga, F. C. Herbert, O. R. Brohlin, A. Shahrivarkevishahi, Y. H. Wijesundara, K. Veera, C. E. Benjamin, S. Popal, M. D. Burton, M. A. Ingersoll, N. J. De Nisco, J. J. Gassensmith, **2021**, https://doi.org/10.1101/2020.06.14.148452.
[26] C. Wang, S. Tadepalli, J. Luan, K. K. Liu, J. J. Morrissey, E. D. Kharasch, R. R. Naik, S. Singamaneni, *Adv. Mater.* **2017**, *29*, 1604433.
[27] P. Horcajada, C. Serre, M. Vallet-Regí, M. Sebban, F. Taulelle, G. Férey, *Angew. Chem., Int. Ed. Engl.* **2006**, *45*, 5974.
[28] M. P. Suh, H. J. Park, T. K. Prasad, D.-W. Lim, *Chem. Rev.* **2012**, *112*, 782.
[29] L. Ma, C. Abney, W. Lin, *Chem. Soc. Rev.* **2009**, *38*, 1248.
[30] K. Liang, C. J. Coghlan, S. G. Bell, C. Doonan, P. Falcaro, *Chem. Commun.* **2016**, *52*, 473.
[31] S. Tadepalli, J. Yim, S. Cao, Z. Wang, R. R. Naik, S. Singamaneni, *Small* **2018**, *14*, 1702382.
[32] F. S. Liao, W. S. Lo, Y. S. Hsu, C. C. Wu, S. C. Wang, F. K. Shieh, J. V. Morabito, L. Y. Chou, K. C. W. Wu, C. K. Tsung, *J. Am. Chem. Soc.* **2017**, *139*, 6530.
[33] X. Wu, J. Ge, C. Yang, M. Hou, Z. Liu, *Chem. Commun.* **2015**, *51*, 13408.
[34] L. E. Gralinski, V. D. Menachery, *Viruses* **2020**, *12*, 135.
[35] J. D. Berry, K. Hay, J. M. Rini, M. Yu, L. Wang, F. A. Plummer, C. R. Corbett, A. Andonov, *mAbs* **2010**, *2*, 53.
[36] K. M. McAndrews, D. P. Dowlatshahi, J. Dai, L. M. Becker, J. Hensel, L. M. Snowden, J. M. Leveille, M. R. Brunner, K. W. Holden, N. S. Hopkins, A. M. Harris, J. Kumpati, M. A. Whitt, J. J. Lee, L. L. Ostrosky-Zeichner, R. Papanna, V. S. LeBleu, J. P. Allison, R. Kalluri, *JCI Insight* **2020**, *5*, e142386.
[37] C. Atyeo, S. Fischinger, T. Zohar, M. D. Slein, J. Burke, C. Loos, D. J. McCulloch, K. L. Newman, C. Wolf, J. Yu, K. Shuey, J. Feldman, B. M. Hauser, T. Caradonna, A. G. Schmidt, T. J. Suscovich, C. Linde, Y. Cai, D. Barouch, E. T. Ryan, R. C. Charles, D. Lauffenburger, H. Chu, G. Alter, *Immunity* **2020**, *53*, 524.
[38] C. Wang, H. Sun, J. Luan, Q. Jiang, S. Tadepalli, J. J. Morrissey, E. D. Kharasch, S. Singamaneni, *Chem. Mater.* **2018**, *30*, 1291.
[39] X. Xu, K. Lin, Y. Wang, K. Xu, Y. Sun, X. Yang, M. Yang, Z. He, Y. Zhang, H. Zheng, X. Chen, *Nanoscale* **2020**, *12*, 16359.
[40] H. Zheng, Y. Zhang, L. Liu, W. Wan, P. Guo, A. M. Nyström, X. Zou, *J. Am. Chem. Soc.* **2016**, *138*, 962.
[41] K. Eum, K. C. Jayachandrababu, F. Rashidi, K. Zhang, J. Leisen, S. Graham, R. P. Lively, R. R. Chance, D. S. Sholl, C. W. Jones, S. Nair, *J. Am. Chem. Soc.* **2015**, *137*, 4191.
[42] S. A. Overman, G. J. Thomas, *Biochemistry* **1998**, *37*, 5654.
[43] Z. Chi, X. G. Chen, J. S. Holtz, S. A. Asher, *Biochemistry* **1998**, *37*, 2854.
[44] D. W. Cleveland, S. G. Fischer, M. W. Kirschner, U. K. Laemmli, *J. Biol. Chem.* **1977**, *252*, 1102.

 